International Journal of Solids and Structures 50 (2013) 147–159

Contents lists available at SciVerse ScienceDirect

International Journal of Solids and Structures

journal homepage: www.elsevier.com/locate/ijsolstr

A numerical approach for equilibrium and stability analysis of slender arches and rings under contact constraints

Ricardo A.M. Silveira [a], Christianne L. Nogueira [b,*], Paulo B. Gonçalves [c]

[a] Department of Civil Engineering, School of Mines, Federal University of Ouro Preto Campus Universitário, Morro do Cruzeiro, 35400-000 Ouro Preto, MG, Brazil
[b] Department of Mines Engineering, School of Mines, Federal University of Ouro Preto Campus Universitário, Morro do Cruzeiro, 35400-000 Ouro Preto, MG, Brazil
[c] Department of Civil Engineering, Pontifical Catholic University, PUC-Rio Rua Marquês de São Vicente, 225, Gávea, 22453-900 Rio de Janeiro, RJ, Brazil

ARTICLE INFO

Article history:
Received 9 February 2012
Received in revised form 6 May 2012
Available online 27 September 2012

Keywords:
Support system
Arches
Rings
Tensionless foundation
Finite element method
Geometric nonlinearity
Unilateral contact

ABSTRACT

Underground constructions, such as shafts, courtain walls, foundations, pipes and tunnels, use structural elements that are supported by a geological medium (soil or rock) or are used to support the geological medium loads. If the geological medium is unable to react under tension, the structural element is subjected to unilateral contact constraints and, during the deformation process, may loose contact with the surrounding medium at one or more regions. The present work proposes an alternative numerical methodology for the geometrically nonlinear analysis of structural systems under unilateral contact constraints. The nonlinear problem involves two different types of variables: the displacement field and the length and position of the contact regions. In order to solve the resulting algebraic nonlinear equations with contact constraints and obtain the structural equilibrium configuration, the present work proposes a two-level iteration solution strategy at each load step. The first solves the contact problem as a linear complementary problem using Lemke's algorithm. The second updates the displacement field. A nonlinear beam-column element is used to model the structure, while a bed of springs is used to model the geological medium. The use of an updated Lagrangian formulation, together with continuation and optimization techniques minimize the errors along the equilibrium paths and enables one to trace convoluted non-linear equilibrium paths with a varying number of contact regions. Special attention is given to the behavior of curved unidimensional support systems such as arches and rings. The nonlinear behavior of four such support systems is studied. The results clarify the influence of the foundation position (above or below the structure) and its stiffness on the nonlinear behavior and stability of curved structures. Comparison of the present results with those found in literature demonstrates the accuracy and versatility of the proposed numerical strategy in the analysis of structural elements with unilateral contact constraints.

1. Introduction

In recent years, there has been a growing interest in underground constructions, especially in big cities, where there is a ground space shortage. Structural elements in these constructions are supported by a geological medium or are used to support the geological medium loads (as in the case of walls and roofs). In many situations, the geological medium is unable to react under tension, and the structure during the deformation process may loose contact with the surrounding medium. Foundation structures, arches, rings and circular or parabolic tunnel roofs are examples of support systems found in civil engineering where unilateral contact may occur. In addition, unilateral contact may occur in several situations involving pipelines and tubular liners. The unilateral contact may lead to important differences in foundation reactions and internal stresses in the structure, causing concentrations of high stresses in the contact region, which are overlooked when traditional bilateral contact foundation models are used in the design. In this type of problem, the location and size of the contact regions are not known *a priori* and constitute the main unknowns of the structural analysis.

Unilateral contact problems have been actively researched since the 1970's (Weitsman, 1970; Stein and Wriggers, 1984; Simo et al., 1986; Nour-Omid and Wriggers, 1986; Joo and Kwak, 1986; Belytschko and Neal, 1991; Kodikara and Moore, 1992; Wriggers and Imhof, 1993; Adan et al., 1994). In most of these works, the contact problems are reformulated in approximation spaces using numerical techniques, such as finite element method (FEM). They generally adopt one of following methodologies to treat the

* Corresponding author. Tel.: +55 31 3559 1780; fax: +55 31 3559 1593.
E-mail addresses: ricardo@em.ufop.br (R.A.M. Silveira), chris@em.ufop.br (C.L. Nogueira), paulo@puc-rio.br (P.B. Gonçalves).

0020-7683/$ - see front matter © 2012 Elsevier Ltd. All rights reserved.
http://dx.doi.org/10.1016/j.ijsolstr.2012.09.015

contact constraints: (i) transforming the contact problem into a minimization problem without constraint. This is done by using the usual formulations of structural mechanics, where an iterative solution procedure must be used and the convergence is not always guaranteed; (ii) using mathematical optimization techniques, where the contact problem solution can be achieved with or without explicit elimination of unilateral constraints. Some of the optimization's techniques used for the contact problem are linear and quadratic programming, recursive quadratic programming or, alternatively, methods for the solution of linear complementary problems (LCP) such as the Dantzig's or Lemke's algorithms (Cottle and Dantzig, 1968; Lemke, 1968).

In the last few years, several papers have been published dealing mainly with the behavior of beams and plates resting on a tensionless foundation. For example, geotechnical applications where the soil-structure interaction is highlighted can be found in Mezaini (2006), Küçükarslan and Banerjee (2005), Maheshwari et al. (2004) and Silva et al. (2001). Recently, many papers were published concerning the nonlinear dynamic response of beams and thin and moderately thick plates resting on a Winkler or Pasternak-type tensionless foundation (Celep et al., 2011; Coşkun et al., 2011; Coşkun, 2010; Hsu, 2009; Yu et al., 2006; Güler and Celep, 2005; Celep and Güler, 2004). Numerical approximations involving the buckling and post-buckling behavior of beams and plates under unilateral contact constraints imposed by elastic foundation appear in several papers (Tzaros and Mistakidis, 2011; Sapountzakis and Kampitsis, 2010; Silveira et al., 2008; Muradova and Stavroulakis, 2006; Shen and Li, 2004; Shen and Yu, 2004; Shen and Teng, 2004; Holanda and Gonçalves, 2003; Silveira and Gonçalves, 2001). Wang et al. (2005) provide a state of the art review for beams and plates on elastic foundation, including soil modeling as well as analytical and numerical possibilities for solving this class of contact problem.

However, little is known on the behavior of curved structural elements such as arches and rings under unilateral contact constraints. The specific problem of a thin, circular ring under uniformly distributed load and radially constrained by a rigid foundation was studied by Silveira and Gonçalves (2001), Kodikara and Moore (1992), Simo et al. (1986), Kyriakides and Youn (1984), Pian and Bucciarelli (1967) and Pian et al. (1967). Buckling resistance of a ring encased in circular rigid cavity under uniform external load was also studied by Li and Guice (1995) and Guice and Li (1994). Based on the finite element method, Lu et al. (1999) calculated the critical buckling loads for externally constrained non-circular rings and for infinitely long circular pipes. Later, these authors also considered a finite length shell under unilateral contact constraint (Lu et al., 2005). Omara et al. (1997) conducted an analytical investigation as well as experimental work to predict the buckling pressure of a thin pipe encased in a rigid oval medium. More recently, Shen (2009) and Shen et al. (2010) studied the postbuckling behavior of functionally graded cylindrical shells resting on elastic foundation under internal pressure.

Contrary to perfect plates and beams, where the the position of the foundation (above or below the structural element) does not influence the results, the present work shows that, when a curved element is analyzed and a deformable foundation is considered, the position of the foundation leads to completely different results, influencing not only the nonlinear equilibrium path but also the stability of the structure. To the knowledge of the authors, no paper has yet been published on support systems like arch-soil foundation where the arch's deflection is prevented from the start by unilateral contact constraints. Sun and Natori (1996), for example, studied an arch in which the unilateral constraints are reached for the first time only during the arch's post-buckling regime. The strength and the stiffness of steel arch tunnel supports used in coal mines were analysed numerical and experimentally in Mitri and Hassani (1990) and Khan et al. (1996), but the unilateral constraints were not considered in the analysis. This is a deficiency in the technical literature, since in many underground constructions; arches and rings have been widely used due to their optimal behavior under pressure loads. In structural engineering, it is well known that arches and rings can support and transmit loads mainly through membrane action. This, coupled with more refined design methodologies, leads to slender but safer structures.

So, the main objective of the paper is to study the influence of the geological medium position (above or below the structural element), here considered as a tensionless elastic medium, and its stiffness on the nonlinear equilibrium path and buckling behavior of some archetypal curved elements, such as arches and rings, and to propose a numerical methodology for the geometrically nonlinear analysis of structural elements with unilateral contact constraints. A geometrically nonlinear beam-column element is used to model the slender structure while a bed of spring that exhibits a sign-dependent force-displacement relationship is used to model the geological medium (Silveira, 1995).

An updated Lagrangian formulation is adopted to follow the system's moviment and the influence of friction in the contact area is ignored. The nonlinear problem involves two different types of variables: the displacement field and the length and position of the contact regions. In order to solve the resulting algebraic nonlinear equations with contact constraints and obtain the structural equilibrium configuration, at each load step, the present work proposes a two-level iteration solution strategy. First, in order to obtain the contact areas between the bodies, the contact equilibrium problem is linearized and treated directly as an optimization problem subject to inequality constraints. The resulting linear complementary problem (LCP) is then solved by Lemke's algorithm (Lemke, 1968). At the second iteration level, Newton's iteration coupled with path-following techniques is employed to obtain the new contact forces and the nonlinear equilibrium configuration (Crisfield, 1991, 1997; Chan, 1988). At this point, the nonlinear equilibrium and constraint equations are checked. If they are satisfied, the optimum solution is obtained; otherwise, the procedure is repeated and improved contact regions and displacements are identified.

In order to verify the proposed numerical solution strategy, four examples are presented. The first one shows the local one-way buckling of confined rings under static distributed loading (Pian and Bucciarelli, 1967; Kyriakides and Youn, 1984; Stein and Wriggers, 1984; Li and Kyriakides, 1991; Kodikara and Moore, 1992; Silveira and Gonçalves, 2001). The following two examples analyze the nonlinear behavior of an arch above and below an elastic foundation (Silveira et al., 2008). The last numerical example studies an arch contact problem in which the unilateral constraints are introduced for the first time only during the arch's post-buckling regime (Sun and Natori, 1996). These results demonstrate the accuracy and versatility of the present numerical strategy in the nonlinear solution of structural elements with unilateral constraints.

2. The structural contact problem

Consider the support system shown in Fig. 1. It consists of an arch and an elastic tensionless foundation. Assume that both bodies may undergo large deflections and rotations but with only small strains that are within the elastic range of the material. Assume also that the contact surface is unbonded and frictionless and the region S_c (Fig. 1c) corresponds to the region where contact is likely to occur, which is not known *a priori*. Consider now that the variables are known for the equilibrium configurations 0, Δt, $2\Delta t, \ldots t$, and that the solution for the adjacent configuration $t + \Delta t$ is required.

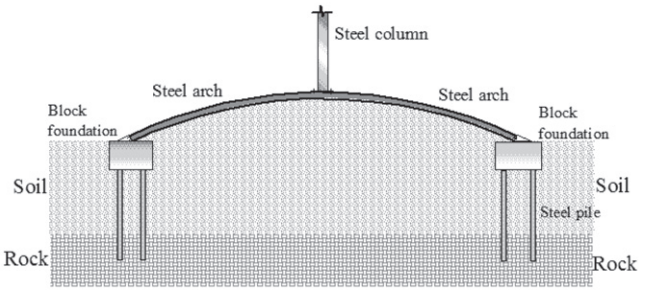

(a) Support system

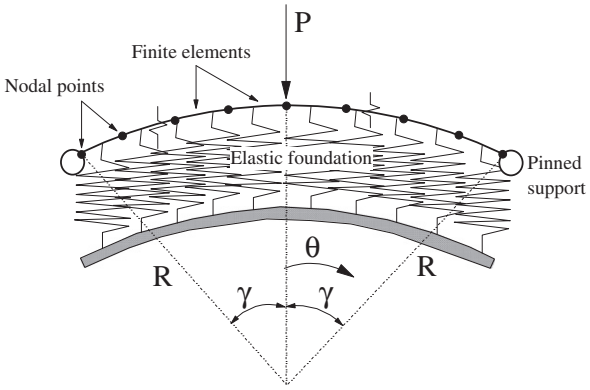

(b) Finite element model

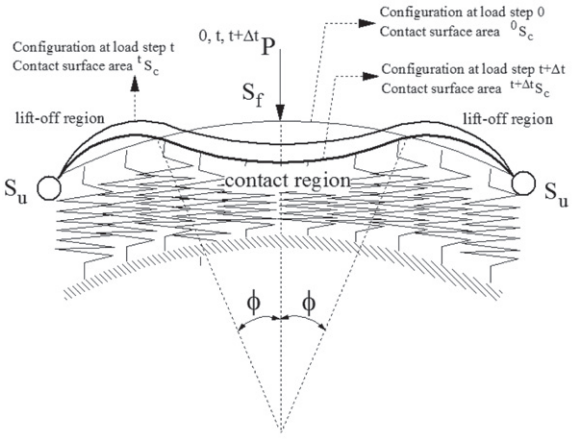

(c) Deformation pattern

Fig. 1. Arch under unilateral contact constraints imposed by an elastic foundation.

Particularly well suited for numerical analysis, the nonlinear contact problem can be solved through the following minimization problem (Joo and Kwak, 1986; Silveira, 1995):

$$\text{Min } \Pi(\Delta\mathbf{u}, \Delta\mathbf{u}_b) \tag{1}$$

$$\text{Subject to}: -\varphi \leqslant 0, \text{ on } S_c \tag{2}$$

with the functional Π written as:

$$\Pi = \int_{tV} ({}^t\boldsymbol{\sigma} + \frac{1}{2}\Delta\mathbf{S})\Delta\boldsymbol{\varepsilon}\, d^tV + \int_{t+\Delta t S_c} ({}^t\mathbf{r}_b + \frac{1}{2}\Delta\mathbf{r}_b)\Delta\mathbf{u}_b\, d^{t+\Delta t}S_c - \int_{t+\Delta t S_f} {}^{t+\Delta t}\mathbf{F}_i\Delta\mathbf{u}_i\, d^{t+\Delta t}S_f \tag{3}$$

in which $\Delta\mathbf{u}$ is the incremental displacements vector of the structure; $\Delta\mathbf{u}_b$ is the incremental displacements vector of the elastic foundation; and $\Delta\boldsymbol{r}_b$ is the incremental compressive reaction vector

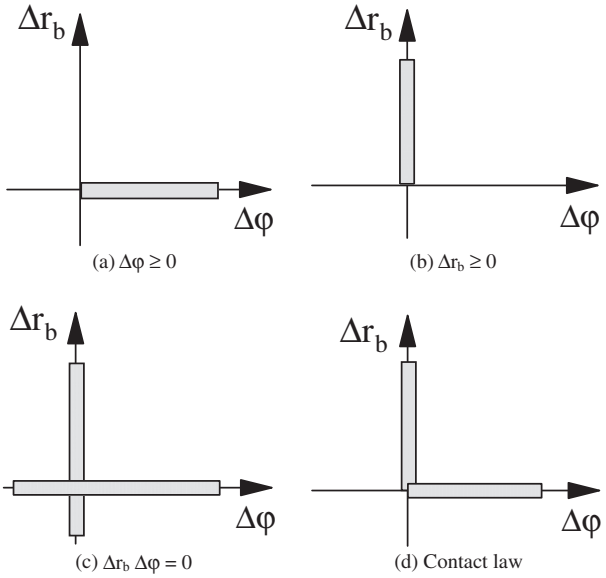

Fig. 2. Domain of validity of the contact constraints.

of the elastic foundation; ${}^t\sigma$ is the Cauchy's stress vector at reference configuration t; and $\Delta\boldsymbol{S}$ is the 2nd Piola-Kirchhoff's stress increment vector. In addition, in Eq. (3), $\Delta\varepsilon_{ij}$ is the increment of the Green-Lagrange's strain vector; and $\boldsymbol{F}_i$ is the external forces vector, specified on S_f and assumed independent of the bodies' deformations.

The inequality (2) gives the contact condition – that is, the gap in the potential contact area – after the increment of the displacements, that must be satisfied on S_c in the configuration $t + \Delta t$. Fig. 2 shows the contact's admissible domains as well as the contact law considered here.

For a given load increment, the unknown variables in the configuration $t + \Delta t$ may be obtained by solving the above minimization problem. The geometrically and contact nonlinear nature of this analysis make the problem difficult to solve directly. The following sections demonstrate how these two kinds of nonlinearities may be treated.

3. Geometrically nonlinear analysis

This section presents the numerical solution process of the geometrically nonlinear problem. The first step is to discretize the structural-geotechnical problem by using the finite element method (Fig. 1b). In this context, one can assume that, for a generic structural element, the incremental displacement field $\Delta\boldsymbol{u}$ within the element is related to the incremental nodal displacements $\Delta\hat{\boldsymbol{u}}$ by:

$$\Delta\boldsymbol{u} = \boldsymbol{H}\Delta\hat{\boldsymbol{u}} \tag{4}$$

where $\boldsymbol{H}$ is the usual FE interpolation functions matrix.

To evaluate the corresponding incremental strains and stresses, one can write the Green-Lagrange increment tensor and the 2nd Piola-Kirchhoff stress increment tensor using the following expressions (Bathe, 1996):

$$\Delta\varepsilon = (\boldsymbol{B}_L + \boldsymbol{B}_{NL})\Delta\hat{\boldsymbol{u}} \tag{5}$$

$$\Delta\boldsymbol{S} = \boldsymbol{C}\Delta\varepsilon \tag{6}$$

where $\boldsymbol{B}_L$ is the same strain-displacement matrix as in the linear infinitesimal strain analysis and it is obtained by appropriately dif-

ferentiating and combining the rows of $\boldsymbol{H}$; $\boldsymbol{B}_{NL}$ depends on $\boldsymbol{H}$ and the incremental displacements; and $\boldsymbol{C}$ is the constitutive matrix.

In many engineering applications, the designer is interested only in the response of the foundation at the contact area and not in the stresses and displacements whitin the foundation. Therefore, it is possible to develop a simple mathematical model to describe, with a reasonable degree of accuracy, the response of the foundation at the contact zone. Using the well-known Winkler model (Kerr, 1964) or the formulation of an elastic half-space (Cheung, 1977), the following discrete equilibrium equation for a generic element can be written to describe the elastic foundation's behavior:

$$\Delta \boldsymbol{r}_b = \boldsymbol{C}_b \Delta \boldsymbol{u}_b \tag{7}$$

where $\Delta \boldsymbol{r}_b$ and $\Delta \boldsymbol{u}_b$ are the incremental elastic foundation reaction and displacement nodal values, respectively; and, $\boldsymbol{C}_b$ is the constitutive matrix of the elastic foundation. Thus, for a generic elastic foundation element, the incremental displacement field $\Delta \boldsymbol{u}_b$ may be related to its nodal values as:

$$\Delta \mathbf{u}_b = \mathbf{B}_b \Delta \hat{\mathbf{u}}_b \tag{8}$$

where $\boldsymbol{B}_b$ is the matrix containing the interpolation functions that describe the elastic base deformation.

Using now the previous definitions and assuming that in the contact area the structure and elastic foundation nodal displacements are identical (i.e., $\Delta \hat{\boldsymbol{u}}_b = \Delta \hat{\boldsymbol{u}}$) one arrives at the discretized functional of the contact problem, Eq. (3), in the local form:

$$\begin{aligned}\bar{\Pi} = {} & \frac{1}{2}\Delta\hat{\boldsymbol{u}}^T \int_{{}^t\bar{V}} \boldsymbol{B}_L^T \boldsymbol{C} \boldsymbol{B}_L \, d^t\bar{V} \, \Delta\hat{\boldsymbol{u}} + \frac{1}{2}\Delta\hat{\boldsymbol{u}}^T \int_{{}^t\bar{V}} (\boldsymbol{B}_L^T \boldsymbol{C} \boldsymbol{B}_{NL} + \boldsymbol{B}_{NL}^T \boldsymbol{C} \boldsymbol{B}_L + \boldsymbol{B}_{NL}^T \boldsymbol{C} \boldsymbol{B}_{NL}) \, d^t\bar{V} \, \Delta\hat{\boldsymbol{u}} \\ & + \Delta\hat{\boldsymbol{u}}^T \int_{{}^t\bar{V}} \boldsymbol{B}_L^T \, {}^t\boldsymbol{\sigma} \, d^t\bar{V} + \Delta\hat{\boldsymbol{u}}^T \int_{{}^t\bar{V}} \boldsymbol{B}_{NL}^T \, {}^t\boldsymbol{\sigma} \, d^t\bar{V} \\ & + \frac{1}{2}\Delta\hat{\boldsymbol{u}}^T \int_{{}^{t+\Delta t}\bar{S}_c} \boldsymbol{B}_b^T \boldsymbol{C}_b \boldsymbol{B}_b \, d^{t+\Delta t}\bar{S}_c \, \Delta\hat{\boldsymbol{u}} + \Delta\hat{\boldsymbol{u}}^T \int_{{}^{t+\Delta t}\bar{S}_c} \boldsymbol{B}_b^T \, {}^t\boldsymbol{r}_b \, d^{t+\Delta t}\bar{S}_c \\ & - \Delta\hat{\boldsymbol{u}}^T \int_{{}^0\bar{S}_f} \boldsymbol{H}^T \, {}^{t+\Delta t}\boldsymbol{F} \, d^0\bar{S}_f \end{aligned} \tag{9}$$

Taking now the appropriate variations of $\bar{\Pi}$ with respect to the incremental nodal displacements, and adding the contributions of each finite element, one can write:

$$[\mathbf{K}_\mathrm{L} + \mathbf{K}_\mathrm{s} + \mathbf{K}_\mathrm{NL} + \mathbf{K}_\mathrm{b}]\Delta\mathbf{U} + {}^\mathrm{t}\mathbf{F}_\mathrm{is} + {}^\mathrm{t}\mathbf{F}_\mathrm{ib} = {}^{\mathrm{t}+\Delta t}\mathbf{R} \tag{10a}$$

or, more concisely:

$${}^{\mathrm{t}+\Delta\mathrm{t}}\mathbf{F}_\mathrm{i} = [\mathbf{K}_\mathrm{L} + \mathbf{K}_\tau + \mathbf{K}_\mathrm{NL} + \mathbf{K}_\mathrm{b}]\Delta\mathbf{U} + {}^\mathrm{t}\mathbf{F}_\mathrm{is} + {}^\mathrm{t}\mathbf{F}_\mathrm{ib} \tag{10b}$$

$${}^{\mathrm{t}+\Delta\mathrm{t}}\mathbf{F}_\mathrm{i}(\Delta\mathbf{U},\mathrm{S_c}) = {}^{\mathrm{t}+\Delta\mathrm{t}}\mathbf{R} \tag{10c}$$

where $\Delta \boldsymbol{U}$ contains the global nodal incremental displacements and ${}^{t+\Delta t}\boldsymbol{F}_i$ is the internal generalised forces vector of the support system in the load step $t + \Delta t$. Eq. (10a) or Eq. (10c) is the equation that must be satisfied in an incremental process to obtain the system equilibrium.

In the left side of (10a), $\boldsymbol{K}_L$ is the global stiffness matrix for small displacement, given by:

$$\boldsymbol{K}_L = \sum_m \int_{{}^t\bar{V}} \boldsymbol{B}_L^T \boldsymbol{C} \boldsymbol{B}_L \, d^t\bar{V} \tag{11}$$

where m is the number of finite elements. The matrix $\boldsymbol{K}_\tau$ is the initial stress matrix or geometric matrix given by:

$$\boldsymbol{K}_\tau = \sum_m \int_{{}^t\bar{V}} \boldsymbol{B}_{NL}^T \, {}^t\boldsymbol{\sigma} \, d^t\bar{V} \tag{12}$$

The matrix $\boldsymbol{K}_{NL}$ is the large displacement matrix, which contains only linear and quadratic terms in the incremental displacement, i.e.:

$$\boldsymbol{K}_{NL} = \sum_m \int_{{}^t\bar{V}} (\boldsymbol{B}_L^T \boldsymbol{C} \boldsymbol{B}_{NL} + \boldsymbol{B}_{NL}^T \boldsymbol{C} \boldsymbol{B}_L + \boldsymbol{B}_{NL}^T \boldsymbol{C} \boldsymbol{B}_{NL}) \, d^t\bar{V} \tag{13}$$

and $\boldsymbol{K}_b$ is the stiffness matrix of the elastic foundation, which is written as:

$$\boldsymbol{K}_b = \sum_{mc} \int_{{}^{t+\Delta t}\bar{S}_c} \boldsymbol{B}_b^T \boldsymbol{C}_b \boldsymbol{B}_b \, d^{t+\Delta t}\bar{S}_c \tag{14}$$

where m_c is the number of elements in the contact region.

The vectors ${}^t\boldsymbol{F}_{is}$ and ${}^t\boldsymbol{F}_{ib}$ represent, respectivaly, the internal force vector of the structure and of the elastic foundation in the equilibrium configuration t. They are typically computed by integrating the generalized stress resultants through the volume of each element and then summing the elemental contributions as follows (Bathe, 1996):

$${}^t\boldsymbol{F}_{is} = \sum_m \int_{{}^t\bar{V}} \boldsymbol{B}_L^T \, {}^t\boldsymbol{\sigma} \, d^t\bar{V} \tag{15a}$$

and

$${}^t\boldsymbol{F}_{ib} = \sum_{mc} \int_{{}^{t+\Delta t}\bar{S}_c} \boldsymbol{B}_b^T \, {}^t\boldsymbol{r}_b \, d^{t+\Delta t}\bar{S}_c \tag{15b}$$

where, again, one considers only the elements in the contact region.

In the right side of (10a), the vector ${}^{t+\Delta t}\boldsymbol{R}$ is the nodal external load vector in the step $t + \Delta t$ and is given by:

$${}^{t+\Delta t}\boldsymbol{R} = \sum_{ms} \int_{{}^0\bar{S}_f} \boldsymbol{H}^T \, {}^{t+\Delta t}\boldsymbol{F} \, d^0\bar{S}_f \tag{16}$$

which is assumed to be independent of the structure's deformation. In the incremental solution strategy, this vector can be more adequately represented as:

$${}^{t+\Delta t}\boldsymbol{R} = {}^{t+\Delta t}\lambda \boldsymbol{R}_r \tag{17}$$

where $\boldsymbol{R}_r$ is a fixed load vector, termed reference vector defining the load direction, and ${}^{t+\Delta t}\lambda$ is a scalar load multiplier which define the intensity of the applied load.

4. Unilateral contact analysis

The support systeḿs analysis taking into account the contact constraint given by Eq. (2) is defined as a non-linear problem because the contact region between the bodies, S_c in Eq. (14) and (15b), is unknown. Several techniques have been used in literature to enforce the unilateral contact constraints. Here, the basic idea is to maintain the unilateral constraints in the formulation, retaining the original philosophy of the problem, by using a mathematical programming approach.

The equilibrium configuration of a conservative system can be obtained from its Lagrange function L as follows:

$$L(\Delta\boldsymbol{u}, \Delta\boldsymbol{u}_b, \mu) = U(\Delta\boldsymbol{u}, \Delta\boldsymbol{u}_b) + V(\Delta\boldsymbol{u}, \lambda) - \int_{S_c} \mu\varphi \, dS_c \tag{18}$$

where U is the internal energy of system, V is the potential of external loads and μ is a Lagrange multiplier used here to take account of the contact constraint, Eq. (2), in Eq. (1).

The Lagrange function L described above is modified by: (1) linearizing the system considering $\boldsymbol{C}\Delta\varepsilon\Delta\varepsilon \cong \boldsymbol{C}\Delta\boldsymbol{e}\Delta\boldsymbol{e}$, where $\Delta\boldsymbol{e}$ is the linear part of the Green-Lagrange strain increment tensor; (2) using the non-discrete form of elastic foundation constitutive relation, Eq. (7); (3) eliminating Δu_b and $\varphi(=\Delta\boldsymbol{u} - \Delta\boldsymbol{u}_b)$ from the analysis; and, (4) finally, by knowing that, physically, the Lagrange multiplier μ must be equal to $\Delta\boldsymbol{r}_b$. These steps lead to the following functional (Silveira, 1995; Ascione and Grimaldi, 1984):

$$L = \frac{1}{2}\int_{tV} \boldsymbol{C}\Delta\boldsymbol{e}\Delta\boldsymbol{e}\, d^tV + \frac{1}{2}\int_{tV} {}^t\boldsymbol{\sigma}\Delta\boldsymbol{\eta}\, d^tV - \frac{1}{2}\int_{S_c} \Delta\boldsymbol{r}_b^T \boldsymbol{D}_b \Delta\boldsymbol{r}_b\, dS_c + \int_{S_c} \Delta\boldsymbol{r}_b \Delta\boldsymbol{u}\, dS_c - \int_{0S_f} {}^{\Delta t}\boldsymbol{F}\Delta\boldsymbol{u}\, d^0S_f \quad (19)$$

with $\mathbf{D}_b = (\mathbf{C}_b)^{-1}$.

Thus, using finite elements to model the support system and adding the contributions of each element, one arrives at the discretized Lagrange function of the problem in the global form:

$$\bar{L} = \frac{1}{2}\Delta\boldsymbol{U}^T\boldsymbol{K}\Delta\boldsymbol{U} - \frac{1}{2}\Delta\boldsymbol{R}_b^T\boldsymbol{T}\Delta\boldsymbol{R}_b + \Delta\boldsymbol{R}_b^T\boldsymbol{A}\Delta\boldsymbol{U} - \Delta\boldsymbol{U}^{T\,\Delta t}\boldsymbol{R} \quad (20)$$

where $\Delta\boldsymbol{R}_b$ is the incremental nodal reaction of the elastic foundation vector and ${}^{\Delta t}\boldsymbol{R}$ is the incremental nodal load vector; $\boldsymbol{K}$ is the linearized tangent stiffness ($\boldsymbol{K}_L + \boldsymbol{K}_\tau$); $\mathbf{A}$ is the joining matrix between the structure and the elastic foundation, which is defined as:

$$\boldsymbol{A} = \sum_{mc}\int_{\bar{S}_c} \boldsymbol{H}_b^T\boldsymbol{H}\, d\bar{S}_c \quad (21)$$

and $\boldsymbol{T}$ is the flexibility matrix of the elastic foundation, which may be written as:

$$\boldsymbol{T} = \sum_{mc}\int_{\bar{S}_c} \boldsymbol{H}_b^T\boldsymbol{D}_b\boldsymbol{H}_b\, d\bar{S}_c \quad (22)$$

where m_c is the number of elements of the contact region.

The first variation of $\bar{L}$ leads to the following variational inequality:

$$\delta\bar{L} = \delta\Delta\boldsymbol{U}^T(\boldsymbol{K}\Delta\boldsymbol{U} + \boldsymbol{A}^T\Delta\boldsymbol{R}_b - {}^{\Delta t}\boldsymbol{R}) + \delta\Delta\boldsymbol{R}_b^T(\boldsymbol{A}\Delta\boldsymbol{U} - \boldsymbol{T}\Delta\boldsymbol{R}_b) \leqslant 0 \quad (23)$$

whose Kuhn-Tucher optimal conditions are related to the following Linear Complementarity Problem (LCP) in terms of the structure displacements and foundation reaction (Silveira, 1995):

$$\boldsymbol{K}\Delta(\boldsymbol{U}) + \boldsymbol{A}^T\Delta\boldsymbol{R}_b - {}^{\Delta t}\boldsymbol{R} \quad (24)$$

$$\boldsymbol{A}\Delta\boldsymbol{U} - \boldsymbol{T}\Delta\boldsymbol{R}_b \leqslant 0;\ \Delta\boldsymbol{R}_b \geqslant 0;\ (\boldsymbol{A}\Delta\boldsymbol{U} - \boldsymbol{T}\Delta\boldsymbol{R}_b)^T\Delta\boldsymbol{R}_b = 0 \quad (25a,b,c)$$

1. Initial state: ${}^t\mathbf{U}$, ${}^t\lambda$, ${}^tS_c$

2. Contact problem iterations: n = 1,2,…, N_c

3. Tangent incremental solution: ${}^n\Delta\lambda^0$ and ${}^n\Delta\mathbf{u}^0$
3.1. Compute: ${}^n\mathbf{K}_t = \mathbf{K}_L + \mathbf{K}_\tau + \mathbf{K}_b$
3.2. Solve: ${}^n\mathbf{K}_t\,\delta\mathbf{U}_t = \mathbf{R}_r$
3.3. Define (Crisfield 1991): ${}^n\Delta\lambda^0 = \pm\Delta\ell / \sqrt{\delta\mathbf{U}_t^T\delta\mathbf{U}_t + \mathbf{R}_r^T\mathbf{R}_r}$
3.4. Compute: ${}^n\Delta\mathbf{U}^0 = {}^n\Delta\lambda^0\,\delta\mathbf{U}_t$
3.5. Updated: ${}^{t+\Delta t}\lambda = {}^t\lambda + {}^n\Delta\lambda^0$ and ${}^{t+\Delta t}\mathbf{U} = {}^t\mathbf{U} + {}^n\Delta\mathbf{U}^0$

4. Solve LC Problem: ${}^{(n)t+\Delta t}S_c^{ini}$
4.1. Compute: matrix ${}^n\mathbf{M}$ and vector ${}^n\mathbf{q}$
4.2. Solve (Lemke 1968): $\mathbf{w} = {}^n\mathbf{q} + {}^n\mathbf{M}\,\Delta\mathbf{r}_b;\ \mathbf{w} \geq \mathbf{0};\ \Delta\mathbf{r}_b \geq \mathbf{0};\ \mathbf{w}^T\Delta\mathbf{r}_b = \mathbf{0}$
4.3. Compute new contact region: $\boxed{{}^{(n)t+\Delta t}S_c^{ini}}$

5. Newton-Raphson iterations: k = 1,2,…,N_i
5.1. Consider now: ${}^{(n)t+\Delta t}S_c^{ini}$
5.2. Compute: ${}^{t+\Delta t}\mathbf{F}_i^{(k-1)} = \left[\mathbf{K}_L + \mathbf{K}_\tau + \mathbf{K}_{NL} + \mathbf{K}_b\right]\Delta\mathbf{U}^{(k-1)} + {}^t\mathbf{F}_{is} + {}^t\mathbf{F}_{ib}$
5.3. Compute: ${}^n\mathbf{g}^{(k-1)} = {}^{t+\Delta t}\mathbf{F}_i^{(k-1)} - {}^{t+\Delta t}\lambda^{(k-1)}\mathbf{R}_r$
5.4. Check convergence: $\left\|{}^n\mathbf{g}^{(k-1)}\right\| / \left\|\Delta\lambda^{(k-1)}\mathbf{R}_r\right\| \leq \xi$

Yes: Go to step 5.7
No: Go to step 5.5
5.5. Compute (Chan 1988): ${}^n\delta\mathbf{U}^k = \delta\mathbf{U}_g^k + {}^n\delta\lambda^k\,\delta\mathbf{U}_r^k$, where,
$\delta\mathbf{U}_g^k = -\mathbf{K}^{-1(k-1)}\,{}^n\mathbf{g}^{(k-1)}$, $\delta\mathbf{U}_r^k = \mathbf{K}^{-1(k-1)}\,\mathbf{R}_r$ and ${}^n\delta\lambda^k = -(\delta\mathbf{U}_r^k)^T\delta\mathbf{U}_g^k / [(\delta\mathbf{U}_r^k)^T\delta\mathbf{U}_r^k]$
5.6. Update:
Incremental: $\Delta\lambda^k = \Delta\lambda^{(k-1)} + {}^n\delta\lambda^k$ and $\Delta\mathbf{U}^k = \Delta\mathbf{U}^{(k-1)} + {}^n\delta\mathbf{U}^k$
Total: ${}^{t+\Delta t}\lambda^k = {}^t\lambda + \Delta\lambda^k$ and ${}^{t+\Delta t}\mathbf{U}^k = {}^t\mathbf{U} + \Delta\mathbf{U}^k$. Return to step 5
5.7. Compute the new contact region: $\boxed{{}^{(n)t+\Delta t}S_c^{new}}$
5.8. Check convergence: ${}^{(n)t+\Delta t}S_c^{new} - {}^{(n)t+\Delta t}S_c^{ini} \leq \zeta_c$
Yes: New load increment. Go to step 1
No: Make ${}^tS_c = {}^{(n)t+\Delta t}S_c^{new}$, change $\mathbf{K}_\tau$ and $\mathbf{K}_b$, updated variables and return to step 2

Notation:
λ, $\Delta\lambda$, $\delta\lambda$ and $\mathbf{U}$, $\Delta\mathbf{U}$, $\delta\mathbf{U}$ = total, incremental and iterative load parameter and nodal displacements; n and k = iteration counters; (k-1) = last iteration; N_c and N_i = maximum iteration numbers; ξ and ζ_c = tolerance; $\mathbf{K}_t$ = tangent stiffness matrix; $\delta\mathbf{U}_t$ = tangent displacement vector; $\delta\mathbf{U}_g$ and $\delta\mathbf{U}_r$ = iterative change in $\mathbf{U}$ due to $\mathbf{g}$ and $\mathbf{R}_r$; $\Delta\ell$ = arch-length; ${}^tS_c$ and ${}^{t+\Delta t}S_c$ = contact region between the bodies in the equilibrium configuration t and t+Δt.

Fig. 3. Proposed numerical nonlinear solution strategy.

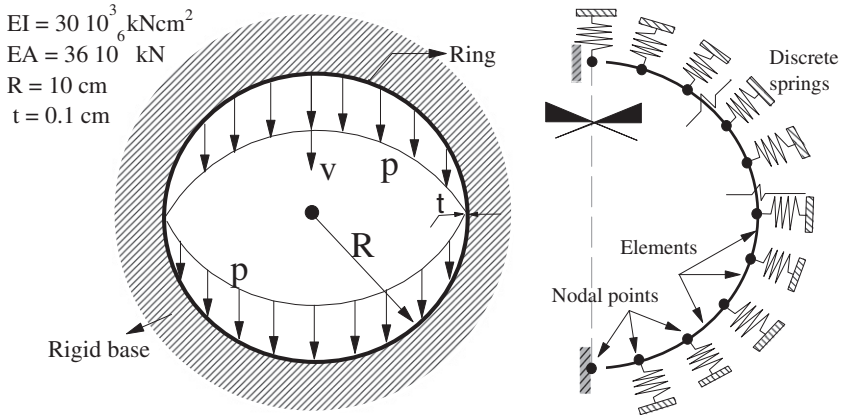

(a) Structural problem (b) Finite element model

Fig. 4. Ring under unilateral constraints imposed by a rigid confinement.

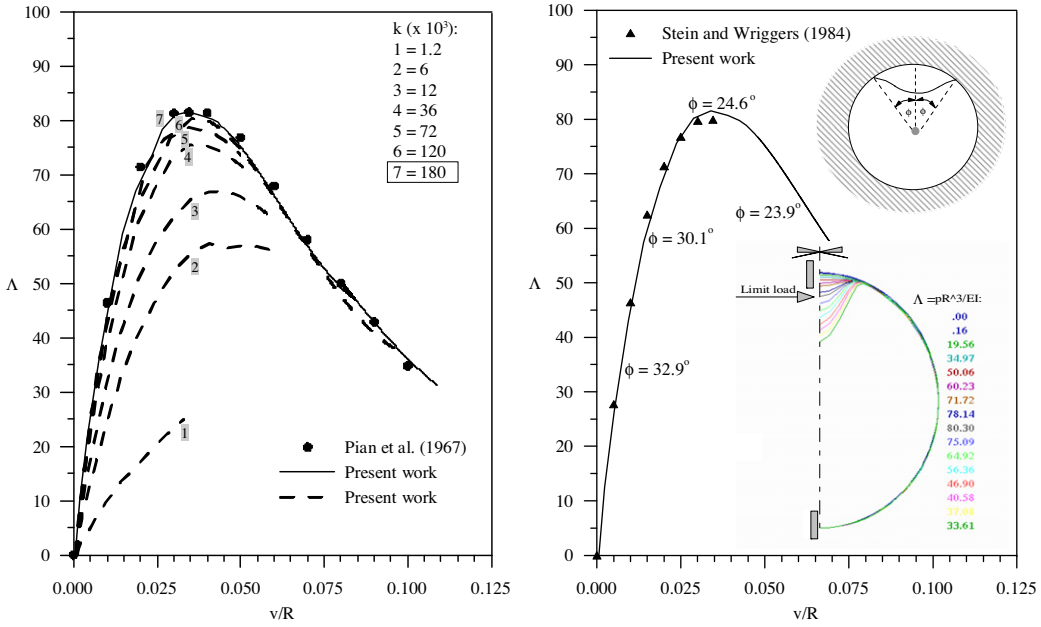

(a) Influence of the base stiffness on nonlinear response (b) Deformation pattern and separation angle ϕ.

Fig. 5. Ring load-deflection curve for inertial loading.

where Eq. (24) is the support system equilibrium equations and Eqs. (25a,b,c) are the constraints that characterise the unilateral contact problem. The constraint (25a) represents the condition of impenetrability between the bodies; (25b) is the positivity condition of $\Delta \boldsymbol{R}_b$; and (25c) is the complementarity relation between the gap and $\Delta \boldsymbol{R}_b$.

A dual and more practical and efficient LCP formulation can be obtained if the stiffness matrix in Eq. (24) is positive definite. In such a case, it is possible to establish the following relationship between $\Delta \boldsymbol{U}$ and $\Delta \boldsymbol{R}_b$:

$$\Delta \boldsymbol{U} = \boldsymbol{K}^{-1}({}^{\Delta t}\boldsymbol{R} - \boldsymbol{A}^T \Delta \boldsymbol{R}_b) \tag{26}$$

Substituting this result in Eq. (20), one arrives at a variational expression that is function of the nodal values of the base reaction $\Delta \boldsymbol{R}_b$ only, that is:

$$\bar{\Pi}_1 = -\frac{1}{2}\Delta \boldsymbol{R}_b^T \boldsymbol{M} \Delta \boldsymbol{R}_b + \Delta \boldsymbol{R}_b^T \boldsymbol{q} - s \tag{27}$$

Table 1
Comparison of critical load parameter, $\Lambda_{cr} = pR^3/EI$.

	Pian et al. (1967)	Stein and Wriggers (1984)	Kodikara and Moore (1992)	Present work
Λ_{cr}	81.5	79.9	81.7	81.5

Table 2
Comparison of separation angle ϕ for different load parameter $\Lambda = pR^3/EI$ levels.

Λ	ϕ Pian et al. (1967)	ϕ (Present work)
34 (s)	32.9°	32.2°
57 (s)	30.1°	28.4°
81.5 (n)	24.6°	24.7°
62 (u)	23.9°	22.6°
28 (u)	27.2°	26.1°

Obs. s = stable configuration; n = neutral configuration; u = unstable configuration.

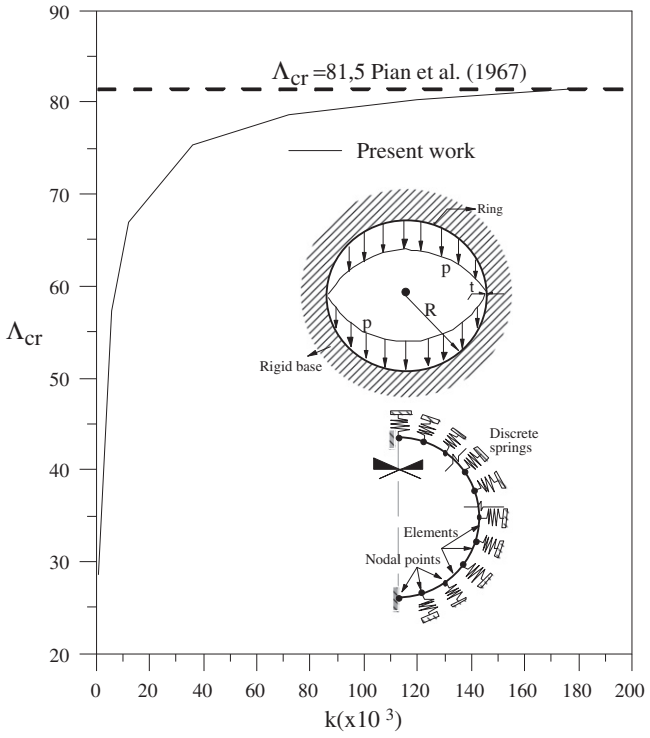

Fig. 6. Variation of the critical limit point load as a function of the foundation stiffness.

Here $\boldsymbol{M}$ is a symmetric positive definite matrix, $\boldsymbol{q}$ is a vector and s is a constant, which are defined as follow:

$$\boldsymbol{M} = \boldsymbol{A}\boldsymbol{K}^{-1}\boldsymbol{A}^T + \boldsymbol{T}; \boldsymbol{q} = \boldsymbol{A}\boldsymbol{K}^{-1\Delta t}\boldsymbol{R}; \mathrm{s} = ({}^{\Delta t}\boldsymbol{R}^T\boldsymbol{K}^{-1\Delta t}\boldsymbol{R})/2 \qquad (28\mathrm{a,b,c})$$

Eq. (27), with the elastic foundation reaction constraint, characterizes the following quadratic programming problem (QPP):

$$\text{Max } \bar{\Pi}_1(\Delta \boldsymbol{R}_b) \qquad (29)$$

$$\text{Subject to}: \Delta \boldsymbol{R}_b \geqslant 0, \text{ on } S_c \qquad (30)$$

Again, considering the Kuhn-Tucker conditions of this QPP, one can derive a LCP similar to that described by Eqs. (24) and (25), where now,

$$\mathbf{w} = \mathbf{q} + \mathbf{M}\Delta\mathbf{R}_b \qquad (31)$$

$$\mathbf{w} \geqslant \mathbf{0}; \Delta\mathbf{R}_b \geqslant 0; \text{and } \mathbf{w}^T\Delta\mathbf{R}_b = 0 \qquad (32,\mathrm{a,bc})$$

and the vector $\boldsymbol{w}$ is the Lagrange multiplier introduced in the analysis to represent the impenetrability condition between the bodies.

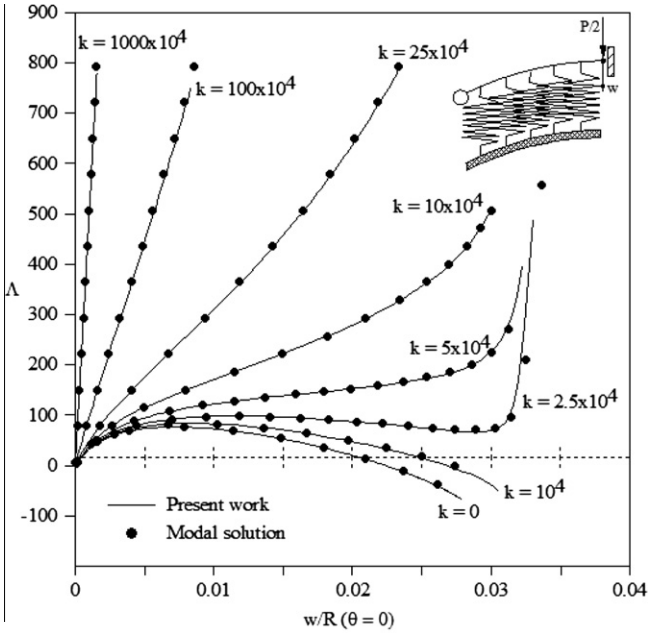

(a) Equilibrium paths for various values of the foundation stiffness k

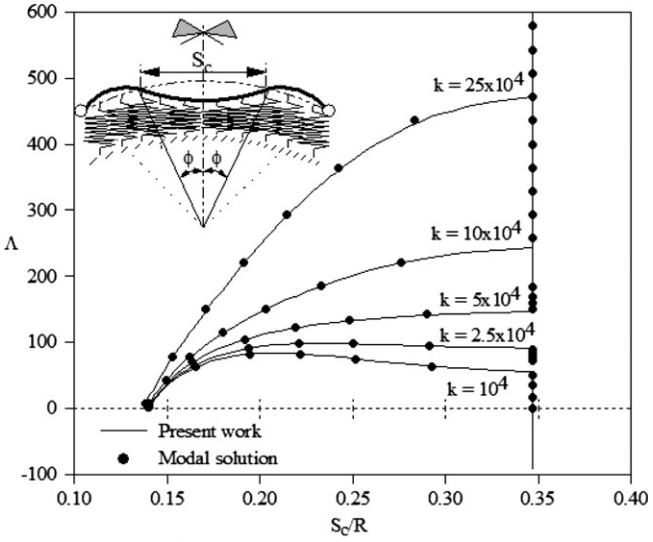

(b) Variation of the contact region S_c

Fig. 8. Equilibrium and stability analysis of the arch above elastic foundation.

After the calculation of $\Delta\boldsymbol{R}_b$, $\Delta\boldsymbol{U}$ can be obtained from Eq. (26). The solution of this LCP can be achieved through mathematical

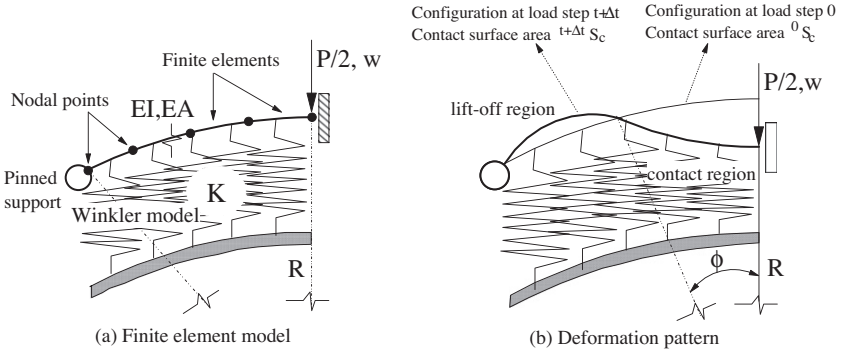

(a) Finite element model (b) Deformation pattern

Fig. 7. Arch under unilateral constraints imposed by an elastic foundation. (Case 1: arch above elastic foundation.)

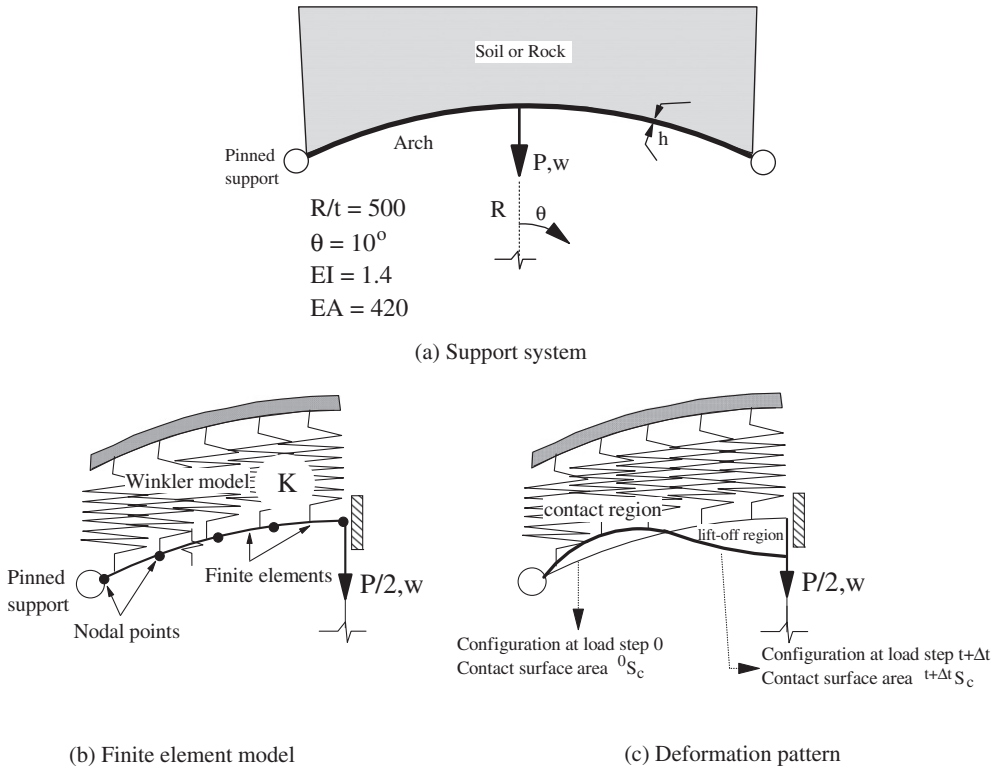

Fig. 9. Arch under unilateral constraints imposed by a tensionless elastic foundation. (Case 2: arch under elastic foundation.)

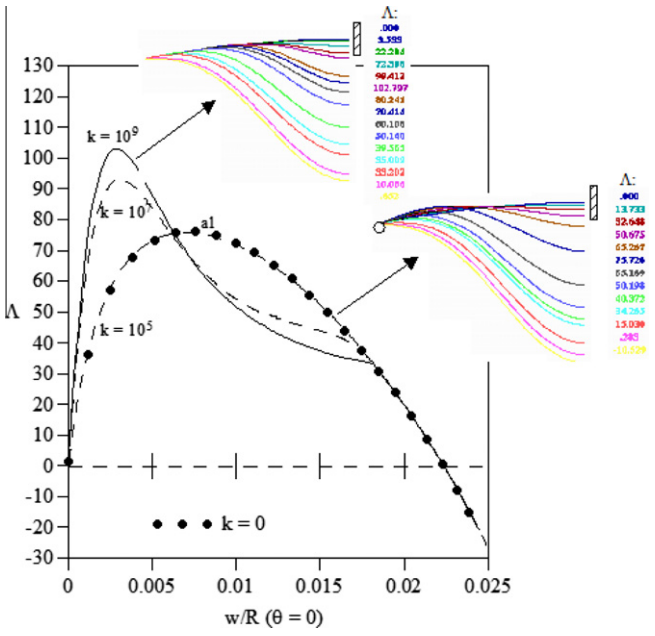

Fig. 10. Nonlinear equilibrium paths of the arch under contact constraints imposed by an elastic foundation (Case 2: arch under elastic foundation).

programming methods, in particular, pivoting techniques developed for complementary problems (Cottle and Dantzig, 1968; Lemke, 1968).

5. Numerical solution procedure

This section presents the main characteristics of the numerical solution strategy adopted for the minimization problem defined by Eq. (1) and (2), considering the geometric nonlinearity and the unilateral contact constraints.

In order to obtain nonlinear equilibrium paths, an incremental-iterative solution strategy is adopted. It is assumed that perfect convergence was achieved in the previous load steps 0, Δt, $2\Delta t, \ldots, t$, i.e., the solution of the previous steps satisfies the equilibrium equations and all contact constraints. Therefore, considering the updated Lagrangian formulation, the known displacements, stresses, and contact region (^tS_c) obtained at the conclusion of load step t are used as information to obtain the adjacent equilibrium configuration $t + \Delta t$. A cycle of the incremental-iterative strategy can be summarized in three steps:

(1) As a starting point, an approximate solution, called a "tangential incremental solution" is used. This approximate solution involves the selection of the initial increment of the load and an estimated contact region between the structure and the elastic foundation. An additional constraint equation, like the 'arch-length' constraint equation (Crisfield, 1991, 1997) may be used to calculate the initial load increment and ^tS_c is assumed to be the contact surface between the bodies. These approximations are employed to calculate the initial increment of the displacements. This 'tangential incremental solution' rarely satisfies both the equilibrium equations and the contact constraints, so the following two corrections are used;

(2) The first correction deals with only the non-linearity associated with the unilateral constraints and is used to correct the dimension of the contact zone, which was assumed to be equal to ^tS_c at the previous step. By solving the unilateral contact problem, described by Eq. (31) and constraint (32), as a linear complementary problem (LCP), an improved solution $^{t+\Delta t}S_c^{ini}$ for the contact regions is obtained;

(3) The second correction deals with the geometric nonlinearity of the problem. Here the Newton-Raphson's method is used

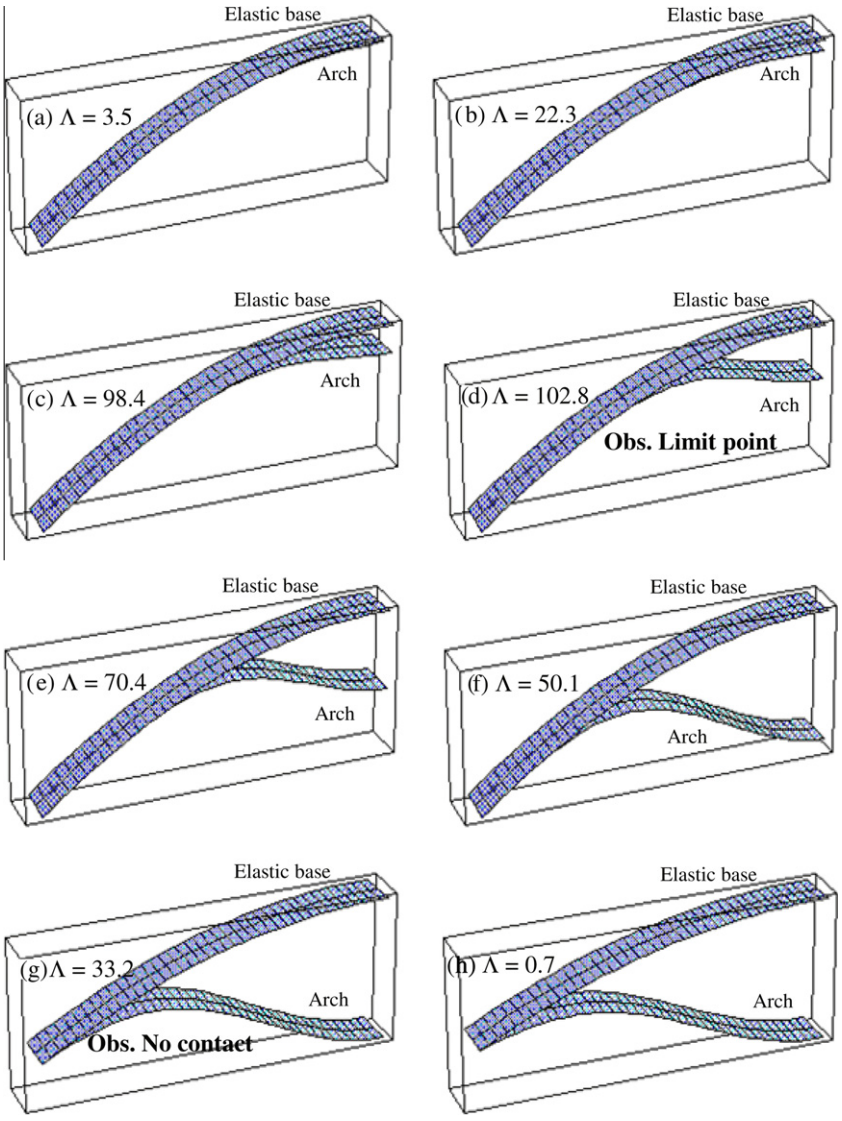

Fig. 11. Arch and elastic foundation deformations for $k = 10^9$ ($\Lambda = PR^2/EI$; scale factor = 10).

to solve the discretized equilibrium equations, correcting the predictor solution. This solution is achieved by using the improved contact solution obtained in the previous step, ${}^{t+\Delta t}S_c^{ini}$, and by coupling path-following techniques (continuation methods) and the Newton-Raphson method. The minimum residual displacement method developed by Chan (1988) is used to allow limit points to be passed and, consequently, to identify snap buckling phenomena. After the converge of the Newton iterative procedure, a new contact region ${}^{t+\Delta t}S_c^{new}$ is obtained and compared with the previous solution, ${}^{t+\Delta t}S_c^{ini}$. If the convergence criterion for the contact zone is not satisfied, a new incremental solution is obtained and the correction procedure is repeated until the convergence criteria are satisfied.

The numerical solution procedure developed here, and summarised above, is better detailed in Fig. 3.

6. Numerical examples

The nonlinear beam-column element developed by Alves (1995), and later improved by Galvão (2000), is adopted to model the structures analyzed in this section. The first three examples involve structures subjected from the start to unilateral contact constraints; the last problem analyzes an arch where the inequality constraints are only imposed in the arch's post-buckling regime. In the proposed numerical solution strategy, the convergence factors $\xi = 10^{-3}$ and $\zeta_c = 10^{-1}$ are adopted and consistent units are used in all examples.

6.1. Circular ring in rigid confinement

The first example used to test the present numerical methodology is illustrated in Fig. 4a. It consists of a radially constrained circular ring of rectangular cross-section under statically applied distributed downward loading p. The surrounding medium is considered a tensionless rigid foundation, so that the ring can only deform inward. The geometrical and physical parameters used in the analysis are also shown in Fig. 4a. Here the ring deforms locally inward and is subjected to limit point instability when the length of the contact region reaches a critical value. Due to symmetry, only a half ring is discretized, as shown in Fig. 4b, and 50 nonlinear beam-column elements are adopted. The rigid foundation is modeled by discrete springs, also illustrated in Fig. 4b.

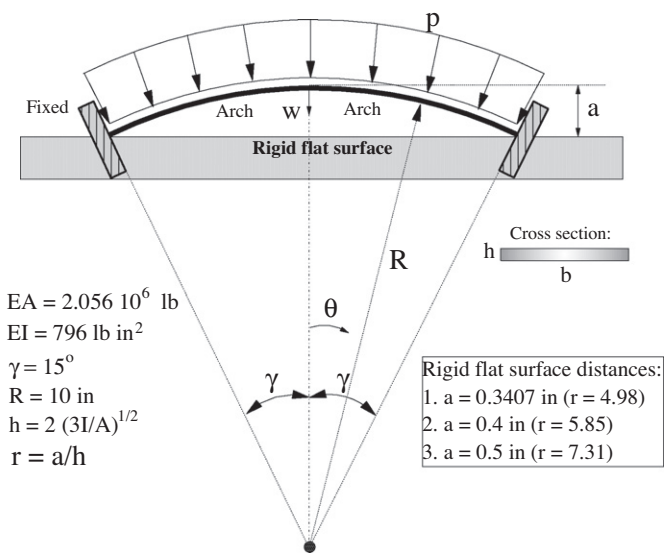

(a) Engineering problem.

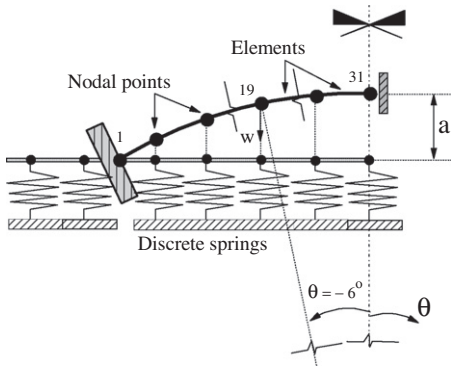

(b) Finite element model.

Fig. 12. Circular arch under radial uniform pressure and contact constraints.

This problem was analyzed previously by Pian et al. (1967) using a finite difference formulation and by Stein and Wriggers (1984) who, using the finite element method, obtained the non-linear equilibrium path up to the critical load. Kodikara and Moore (1992) also studied the same ring using a FE model (48 curved cubic isoparametric elements for a half ring) and a general nonlinear iteration approach for the numerical treatment of solids with rigid surfaces.

The results obtained by these researchers, showing the variation of the non-dimensional load parameter $\Lambda = pR^3/EI$ with the deflection of the point lying on the vertical axis of symmetry v divided by R, are compared with the results of the present numerical formulation in Fig. 5a and b. Their values for the critical load parameter are better compared with the present result in Table 1. Notice that after reaching the upper limit point, the ring under increasing load jumps to a remote attractor associated with large displacements and rotations (snap-through buckling). The response beyond the limit load is unstable until the crown of the ring touches the opposite side. The computed values of the separation angle φ at different load levels, corresponding to stable, neutral and unstable configurations, are compared to those reported by Pian et al. (1967) in Table 2. At the limit point, $\varphi = 24.7°$ ($\varphi = 24.6°$ in Pian et al. (1967) and $\varphi = 24°$ in Stein and Wriggers (1984)). As observed, the present results compare well with those found in the literature. This type of collapse is often observed in the

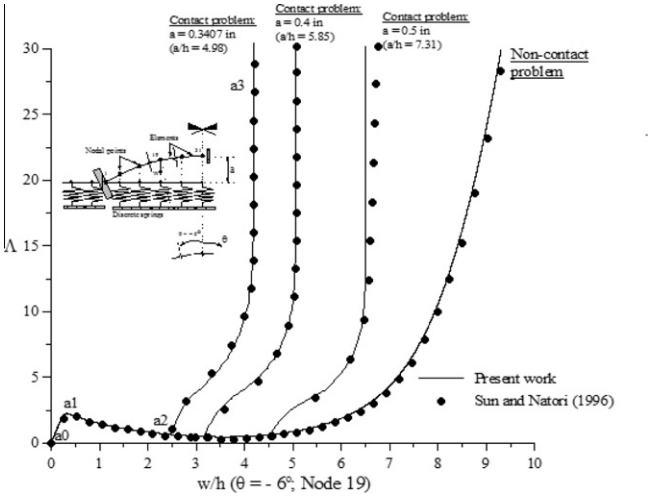

Fig. 13. Load-displacement curves of the circular arch under radial uniform pressure and contact constraints.

liners of stiff cavities such as grouted oil-well casing (Kyriakides and Lee, 2005).

In many applications, however, the ring is embedded in a soft soil. In order to investigate the influence of the foundation stiffness on the non-linear response and the stability of the ring, the system was analyzed considering increasing values for the non-dimensional elastic foundation stiffness parameter $k = KR^3/EI$ (discrete spring). The results are also presented in Fig. 5a. As the foundation's stiffness increases the limit point load increases and the results approach asymptotically from below those obtained considering a rigid foundation, as shown in Fig. 6, where the limit point load parameter $\Lambda = pR^3/EI$ is plotted as a function of the foundation stiffness parameter $k = KR^3/EI$. A foundation stiffness of $k \cong 180 \times 10^3$ practically reproduces the non-linear response obtained by Pian et al. (1967). It should be pointed out that the use of an elastic foundation with very large stiffness (much higher than $k \cong 180 \times 10^3$ in the present analysis), for example, $k > 12000 \times 10^3$, leads to numerical difficulties and the response presents spurious results and oscillations. This is a problem typical of penalty-type methods, so care should be taken in choosing the foundation stiffness to represent a rigid foundation.

6.2. Arch analysis: elastic foundation below the structure

Consider now the support system shown in Fig. 1. The structure is a slender circular arch of radius R, length $2\gamma R$, bending stiffness EI and membrane stiffness EA resting on a Winkler tensionless elastic foundation of modulus K. Only half arch is discretized as illustrated in Fig. 7a and, for an incremental concentrated load P applied at $\theta = 0$, the expected deformation pattern is shown in Fig. 7b, where a central contact region defined by the angles $\pm\varphi$, is expected, separating too non-contact regions.

The arch's nonlinear equilibrium path without the elastic foundation ($k = 0$) was originally obtained by Walker (1969), considering the data $R/h = 500$ (h = thickness), $\gamma = 10°$, $EI = 1.4$, $EA = 420$,

Table 3
Comparison of critical load parameter Λ_{cr} (phR^2/EI) and the central displacement parameter w_{cr}/h of shallow arch (snap-through behavior).

References	Λ_{cr}	w_{cr}/h
Present work	2.2682	0.8514
Sun and Natori (1996)	2.2784	0.8702
Carnoy (1980)	2.2659	0.8605
Kerr and Soifer (1969)	2.2613	0.8508

with the arch exhibiting a snap-through behavior and a limit load parameter $\Lambda_{lim} = PR^2/EI = 76.21$. The authors of the present paper also solved the same arch resting on a tensionless foundation using a novel semi-analytical approach for unilateral contact problems based on the Ritz method (Silveira et al., 2008).

Thus, the results obtained from this modal analysis are used here to validate the results given by the proposed numerical formulation. These results are compared in Fig. 8a and b. In Fig. 8a, the variation of the lateral displacement w is plotted as a function of the load parameter $\Lambda = PR^2/EI$, for different values of the non-dimensional elastic foundation stiffness parameter $k = KR^4/EI$. Note that for a flexible foundation ($k < 10^4$), no additional effects were observed in the pre- and post-buckling behavior, being the response similar to that of an unconstrained arch. With $k = 10^4$, a small increase in the limit load is observed ($\Lambda_{lim} \cong 83.4$). For $k \geqslant 5 \times 10^4$, the snap-through behavior disappears, and for $k = 100 \times 10^4$ and 1000×10^4 the equilibrium paths are practically linear (very stiff foundation). Fig. 8b displays the variation of contact regions S_c ($2R\varphi$) with the applied load.

6.3. Arch analysis: elastic foundation above the structure

Consider the same structural system as in the last example but now with the elastic foundation located above of the arch, as shown in Fig. 9a. Again, due to the problem symmetry, only half arch is discretized, as shown in Fig. 9b. Fig. 9c shows the deformation pattern of the arch under a concentrated load P applied at = 0, where a central non-contact region is expected. Figs. 10 and 11 present the results obtained for this contact problem using the proposed numerical methodology.

Fig. 10 presents the influence of the non-dimensional elastic foundation stiffness parameter $k = KR^4/EI$ in the arch's nonlinear behavior. Four different values of k are considered, namely: 0, 10^5, 10^7 and 10^9. These relations define various levels of the elastic base stiffness: inexistent ($k = 0$), flexible, semi-rigid and rigid, respectively. For an elastic foundation with $k = 10^5$, the arch's nonlinear equilibrium path is almost the same as in the case of the arch without foundation. The limit load is $\Lambda_{lim} = PR^2/EI \cong 76.1$. As the foundation stiffness increases, the load carrying capacity of the arch increases, accompanied by a decreasing transversal deflection. For $k = 10^7$, for example, the critical load increases to $\Lambda \cong 93$, and for $k = 10^9$, to $\Lambda \cong 103$. Higher values of k were tested but the limit load $\Lambda \cong 103$ was never exceeded, showing that the rigid condition was reached. Fig. 11 shows the variation of the arch deformation pattern along the nonlinear equilibrium path when in contact with a rigid base ($k = 10^9$). All equilibrium paths converge at large deflections to the unconstrained solution as the entire arch looses contact with the foundation. For the three-foundation stiffness relations considered, at the instant of total loss of contact between the bodies the load parameter value is close to $\Lambda \cong 30$. This corresponds to an unstable equilibrium configuration. The comparison of the present results with those of the previous example show that, in the analysis of curved elements, the position of the foundation (above or below the structure) has a strong influence on the nonlinear behavior and buckling load of the structure. Thus, even for straight structural elements, such as plates and beams, when initial geometric imperfections are considered, the direction of the imperfection may change completely the response of the structure.

6.4. Arch analysis: post-buckling contact constraints

The last example, shown in Fig. 12a, considers the nonlinear behavior of a slender circular arch under uniform radial pressure. Researchers have frequently used this arch's buckling and post-buckling responses without contact constraints to test their geometrically nonlinear formulations (Alves, 1995; Kerr and Soifer, 1969; Carnoy, 1980). Sun and Natori (1996) introduced to the analysis the unilateral contact constraints using a rigid flat surface placed in such a way that contact only occurs in the post-critical range. Their finite element results for the perfect arch (symmetrical deformation) behavior are thus used here to validate the proposed numerical formulation.

The finite element model adopted to solve this problem is given in Fig. 12b. Due to the symmetry of the problem, only half the arch is discretized and 30 elements used. The rigid flat surface is

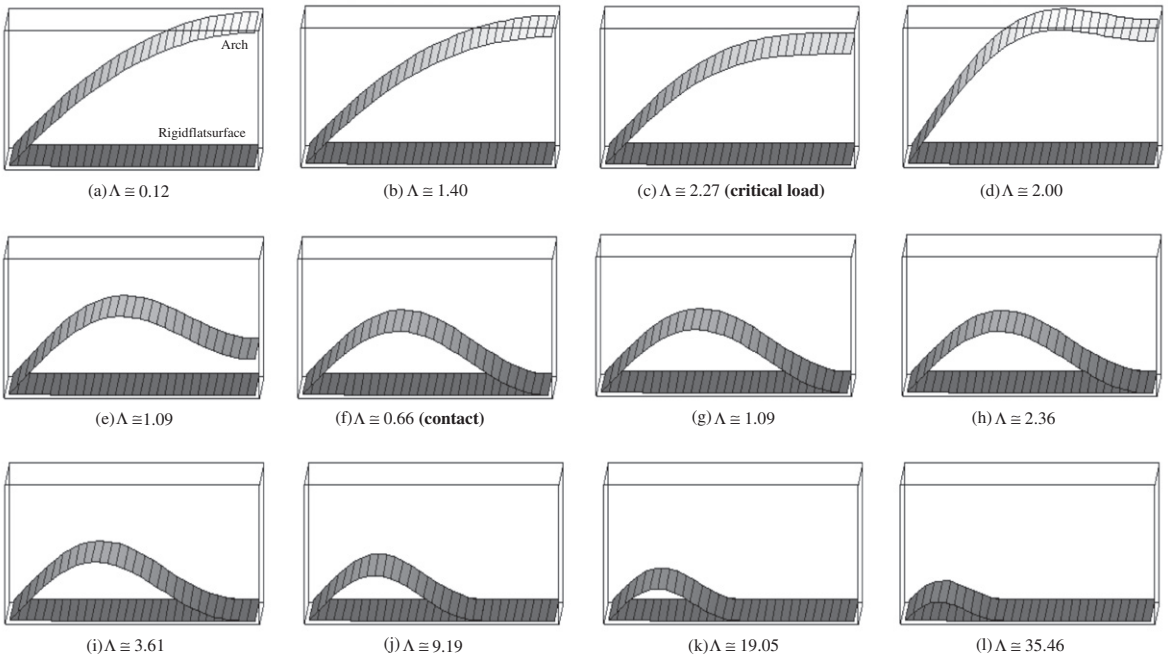

Fig. 14. Arch deformations with contact constraints ($r = a/h = 498$; $\Lambda = phR^2/EI$; scale factor = 10). (a) $\Lambda \cong 0.12$, (b) $\Lambda \cong 1.40$, (c) $\Lambda \cong 2.27$ **(critical load)**, (d) $\Lambda \cong 2.00$, (e) $\Lambda \cong 1.09$, (f) $\Lambda \cong 0.66$ **(contact)**, (g) $\Lambda \cong 1.09$, (h) $\Lambda \cong 2.36$, (i) $\Lambda \cong 3.61$, (j) $\Lambda \cong 9.19$, (k) $\Lambda \cong 19.05$, (l) $\Lambda \cong 35.46$.

described by discrete springs with a high stiffness value. The relative position of the flat surface with regard to the structure's unloaded position is included in the constraint equation.

The equilibrium paths that characterize the nonlinear structural system response are shown in Fig. 13. The variation of the vertical displacement w of node 19 ($\theta = -6^o$) is plotted as a function of the non-dimensional load parameter, $\Lambda = phR^2/EI$. The adopted non-dimensional distance (a/h) between the structure and rigid foundation are 4.98, 5.85 and 7.31. In all cases there is excellent agreement between the present results and those obtained by Sun and Natori (1996), confirming the accuracy and efficiency of the present methodology. Table 3 shows the computed critical load as well as the arch's central vertical displacement obtained using different formulations.

Still looking at Fig. 13, observe that the points $a0$–$a3$ for the contact problem $a/h = 4.95$ indicate transitions between characteristic stages of response. The first part of the equilibrium curve ($a0$–$a1$) follows the familiar nonlinear path of a perfect arch under compression without contact. Contact occurs at position $a2$ ($\Lambda \cong 0.67$). After this point ($a2$–$a3$), as the load increases, the contact region increases with the arch deformation pattern exhibiting a flat central region. The variation of the deformation pattern for increasing load levels is illustrated in Fig. 14, where the configurations corresponding to points $a2$ and $a3$ are identified. As expected, the constrained response is considerably stiffer than the free one.

7. Conclusions

The present work proposes a new numerical strategy for the nonlinear equilibrium and stability analysis of slender curved elements such as arches, pipes and rings under unilateral constraints. An essential step for the success of the proposed numerical algorithm is the linearization of the contact problem at each load increment and its solution as a linear complementary problem (LCP) by using Lemke's algorithm. This linearization, in combination with the use of an updated Lagrangian formulation, continuation methods and an efficient incremental-iterative strategy allows the simultaneous calculation of the two problem variables: the size and location of the contact regions and the displacement fields. The iterative procedure minimizes the errors along the equilibrium path and enables one to trace convoluted non-linear equilibrium paths with a varying number of contact regions. In addition, the paper shows that the use of optimization techniques allows for the development of numerically simple algorithms for the solution of non-classical equilibrium and stability problems. Finally, the present formulation can be easily extended to allow the nonlinear analysis of plates and shells under unilateral constraints.

The response of different types of structure-elastic foundation contact problems shows good agreement with those found in literature using different methodologies. The examples analyzed also show that the proposed nonlinear formulation can be used successfully in many engineering problems with the unilateral contact constraints being imposed at the beginning or along the structure deformation process. In addition, the present work clarifies the influence of the foundation position (above or below the structure) and its stiffness on the nonlinear behavior and stability of curved structures. Therefore, engineers can use the proposed methodology for the design of several soil-structure interaction problems, in particular those involving non-cohesive soils.

Acknowledgments

The authors are grateful for the financial support of the Brazilian National Council for Scientific and Technological Development (CNPq/MCT), Coordinating Agency for Advanced Training of High-Level Personnel – Brazil (CAPES) and Minas Gerais and Rio de Janeiro State Foundations (FAPEMIG and FAPERJ). Special thanks also to Professor Michael Engelhardt and Professor Jorge Zornberg, both from University of Texas at Austin, for their hospitality during the manuscript's preparation. We also acknowledge Prof. John White and Harriet Reis for the editorial review of this text.

References

Adan, N., Sheinman, I., Altus, E., 1994. Post-buckling behaviour of beams under contact constraints. Journal of Applied Mechanics (ASME) 61 (4), 764–772.
Alves, R.V., 1995. Non-Linear Elastic Instability of Space Frames. D.Sc. Thesis, Universidade Federal do Rio de Janeiro, UFRJ-COPPE, Portuguese.
Ascione, L., Grimaldi, A., 1984. Unilateral contact between a plate and an elastic foundation. Meccanica 19 (3), 223–233.
Bathe, K.J., 1996. Finite Element Procedures. Prentice-Hall, New Jersey.
Belytschko, T., Neal, M.O., 1991. Contact-impact by the pinball algorithm with penalty and Lagrangian methods. International Journal for Numerical Methods in Engineering 31 (3), 547–572.
Carnoy, E., 1980. Postbuckling analysis of elastic structures by the finite element method. Computer Method in Applied and Mechanic Engineering 23 (2), 143–174.
Celep, Z., Güler, K., 2004. Static and dynamic responses of a rigid circular plate on a tensionless Winkler foundation. Journal of Sound and Vibration 276 (1–2), 449–458.
Celep, Z., Güler, G., Demir, F., 2011. Response of a completely free beam on a tensionless Pasternak foundation subjected to dynamic load. Structural Engineering and Mechanics 37 (1), 61–77.
Chan, S.L., 1988. Geometric and material nonlinear analysis of beam-columns and frames using the minimum residual displacement method. International Journal for Numerical Methods in Engineering 26 (12), 2657–2669.
Cheung, Y.K., 1977. Beams, slabs, and pavements. In: Desai, C.S., Christian, J.T. (Eds.), Numerical Methods in Geotechnical Engineering. McGraw-Hill, New York, pp. 176–210.
Coşkun, I., 2010. Dynamic contact response of a finite beam on a tensionless Pasternak foundation under symmetric and asymmetric loading. Structural Engineering and Mechanics 34 (3), 319–334.
Coşkun, I., Engin, H., Tekin, A., 2011. Dynamic response of a Timoshenko beam on a tensionless Pasternak foundation (Review). Structural Engineering and Mechanics 37 (5), 489–507.
Cottle, R.W., Dantzig, G.B., 1968. Complementary pivot theory of mathematical programming. Linear Algebra and its Applications 1 (1), 103–125.
Crisfield, M.A., 1991. Non-Linear Finite Element Analysis of Solids and Structures, vol. 1. John Wiley & Sons, Chichester, UK.
Crisfield, M.A., 1997. Non-Linear Finite Element Analysis of Solids and Structures, vol. 2. John Wiley & Sons, Chichester, UK.
Galvão, A.S., 2000. Non Linear Finite Element Formulations for Steel Frame Analysis. M.Sc. Thesis, Universidade Federal de Ouro Preto, PROPEC, Portuguese.
Guice, L.K., Li, J.Y., 1994. Buckling models and influencing factors for pipe rehabilitation design. In: Proceedings of the North American NO-DIG '94, Dallas, Texas.
Güler, K., Celep, Z., 2005. Response of a rectangular plate-column system on a tensionless Winkler foundation subjected to static and dynamic loads. International Journal of Structural Engineering and Mechanics 21 (6), 699–712.
Holanda, A.S., Gonçalves, P.B., 2003. Post-buckling analysis of plates resting on a tensionless elastic foundation. Journal of Engineering Mechanics (ASCE) 129 (4), 438–448.
Hsu, M.-H., 2009. Vibration analysis of non-uniform beams resting on elastic foundations using the spline collocation method. Tamkang Journal of Science and Engineering 12 (2), 113–122.
Joo, J.W., Kwak, B.M., 1986. Analysis and applications of elasto-plastic contact problems considering large deformation. Computers and Structures 24 (6), 953–961.
Kerr, A.D., Soifer, M.J., 1969. The linearization of the prebuckling state and its effect on the determined instability loads. Journal of Applied Mechanics 36, 775–783.
Kerr, A.D., 1964. Elastic and viscoelastic foundation models. Journal of Applied Mechanics (ASME) 31, 491–498.
Khan, U.H., Mitri, H.S., Jones, D., 1996. Full scale testing of steel arch tunnel supports. International Journal for Rock Mechanics, Mining Science and Geomechanics Abstract 33 (3), 219–232.
Kodikara, J.K., Moore, I.D., 1992. Nonlinear interaction o solids with rigid surfaces. Computers and Structures 43 (1), 85–91.
Küçükarslan, S., Banerjee, P.K., 2005. Inelastic dynamic analysis of pile-soil-structure interaction. International Journal on Computational Engineering Science 5 (1), 245–258.
Kyriakides, S., Youn, S.-K., 1984. On the collapse of circular confined rings under external pressure. International Journal of Solids and Structures 20 (7), 699–713.
Lemke, C.E., 1968. N complementary pivot theory. Mathematics of Decision Sciences 8, 95–114.
Li, J.Y., Guice, L.K., 1995. Buckling of encased elliptic thin ring. Journal of Engineering Mechanics (ASCE) 121 (12), 1325–1329.

Li, F.-S., Kyriakides, S., 1991. On the response and stability of two concentric, contacting rings under external pressure. International Journal of Solids and Structures 27 (1), 1–14.
Kyriakides, S., Lee, L.-H., 2005. Buckle propagation in confined steel tubes. International Journal of Mechanical Sciences 47 (4–5), 603–620.
Lu, H., Feng, M., Lark, R.J., Williams, F.W., 1999. The calculation of critical buckling loads for externally constrained structures. Communications in Numerical Methods in Engineering 15 (3), 193–201.
Lu, H., Hou, J., Williams, F.W., 2005. Calculation of critical buckling loads for finite length externally constrained thin circular cylinders. Communications in Numerical Methods in Engineering 21 (5), 259–267.
Maheshwari, P., Chandra, S., Basudhar, P.K., 2004. Response of beams on a tensionless extensible geosynthetic-reinforced earth bed subjected to moving loads. Computers and Geotechnics 31 (7), 537–548.
Mezaini, N., 2006. Effects of soil-structures interactions on the analysis of cylindrical tanks. Practice Periodical on Structural Design and Construction (ASCE) 11 (1), 50–57.
Mitri, H.S., Hassani, F.P., 1990. Structural characteristics of coal mine steel arch supports. International Journal for Rock Mechanics, Mining Science and Geomechanics Abstract 27 (2), 121–127.
Muradova, A.D., Stavroulakis, G.E., 2006. A unilateral contact model with buckling in von Kármán plates. Nonlinear Analysis: Real World Applications. http://dx.doi.org/10.1016/j.nonrwa.2006.02.009.
Nour-Omid, B., Wriggers, P., 1986. A two-level iteration method for solution of contact problems. Computer Methods in Applied Mechanics and Engineering 54 (2), 131–144.
Omara, A.M., Guice, L.K., Straughan, W.T., Akl, F.A., 1997. Instability of thin pipes encased in oval rigid cavity. Journal of Engineering Mechanics (ASCE) 126 (4), 381–388.
Pian, T.H.H., Balmer, H.A., Bucciarelli, L.L., 1967. Dynamic buckling of a circular ring constrained in a rigid circular surface. In: Dynamic Stability of Structures. Pergamon Press, Oxford, pp. 285–297.
Pian, T.H.H., Bucciarelli Jr., L.L., 1967. Buckling of a radially constrained circular ring under distributed loading. International Journal of Solids and Structures 3 (5), 715–730.
Sapountzakis, E.J., Kampitsis, A.E., 2010. Nonlinear analysis of shear deformable beam-columns partially supported on tensionless Winkler foundation. International Journal of Engineering, Science and Technology 2 (4), 31–53.
Shen, H.-S., Li, Q.S., 2004. Postbuckling of shear deformable laminated plates resting on a tensionless elastic foundation subjected to mechanical or thermal loading. International Journal of Solids and Structures 41 (16–17), 4769–4785.
Shen, H.-S., Teng, J.G., 2004. Postbuckling analysis of unilaterally constrained laminated thin plates. Composite Structures 66 (1–4), 571–578.
Shen, H.-S., 2009. Postbuckling of shear deformable FGM cylindrical shells surrounded by an elastic medium. International Journal of Mechanical Sciences 51 (5), 372–383.
Shen, H.-S., Yu, L., 2004. Nonlinear bending behavior of Reissner-Mindlin plates with free edges resting on tensionless elastic foundations. International Journal of Solids and Structures 41 (16–17), 4809–4825.
Shen, H.-S., Yang, J., Kitipornchai, S., 2010. Postbuckling of internal pressure loaded FGM cylindrical shells surrounded by an elastic medium. European Journal of Mechanics – A/Solids 29 (3), 448–460.
Silva, A.R.D., Silveira, R.A.M., Gonçalves, P.B., 2001. Numerical methods for analysis of plates on tensionless elastic foundations. Internationanl Journal of Solids and Structures 38 (10–13), 2083–2100.
Silveira, R.A.M., Gonçalves, P.B., 2001. Analysis of slender structural elements under unilateral contact constraints. International Journal Structural Engineering and Mechanics 12 (1), 35–50.
Silveira, R.A.M., Pereira, W.L.A., Gonçalves, P.B., 2008. Nonlinear analysis of structural elements under unilateral contact constraints by a Ritz type approach. International Journal of Solids and Structures 45 (9), 2629–2650.
Silveira, R.A.M., 1995. Analysis of Slender Structural Elements Under Unilateral Contact Constraints. D.Sc. Thesis, Pontifícia Universidade Católica do Rio de Janeiro, PUC-Rio, Portuguese.
Simo, J.C., Wriggers, P., Schweizerhof, K.H., Taylor, R.L., 1986. Finite deformation post-buckling analysis involving inelasticity and contact constraints. International Journal for Numerical Methods in Engineering 23 (23), 779–800.
Stein, E., Wriggers, P., 1984. Stability of rods with unilateral constraints, a finite element solution. Computers and Structures 19 (1–2), 205–211.
Sun, S.M., Natori, M.C., 1996. Numerical solution of large deformation problems involving stability and unilateral constraints. Computers and Structures 58 (6), 1245–1260.
Tzaros, K.A., Mistakidis, E.S., 2011. The unilateral contact buckling problem of continuous beams in the presence of initial geometric imperfections: an analytical approach based on the theory of elastic stability. International Journal of Non-Linear Mechanics 46 (9), 1265–1274.
Walker, A.C., 1969. A non-linear finite element analysis of shallow circular arches. International Journal of Solids and Structures 5 (1), 97–107.
Wang, Y.H., Tham, L.G., Cheung, Y.K., 2005. Beams and plates on elastic foundations: a review. Progress in Structural Engineering and Materials 7 (4), 174–182.
Weitsman, Y., 1970. On foundations that react in compression only. Journal of Applied Mechanics 37, 1019–1030.
Wriggers, P., Imhof, M., 1993. On the treatment of nonlinear unilateral contact problems. Archive of Applied Mechanics 63 (2), 116–129.
Yu, L., Shen, H.-S., Huo, X.-P., 2006. Dynamic responses of Reissner-Mindlin plates with free edges resting on tensionless elastic foundations. Journal of Sound and Vibration. http://dx.doi.org/10.1016/j.jsv.2006.07.015.